Monthly Notices
of the
ROYAL ASTRONOMICAL SOCIETY

MNRAS **460,** 3305–3315 (2016)
Advance Access publication 2016 May 20

doi:10.1093/mnras/stw1217

The *Gaia*-ESO Survey: pre-main-sequence stars in the young open cluster NGC 3293⋆

A. J. Delgado,[1]† L. Sampedro,[1] E. J. Alfaro,[1] M. T. Costado,[1] J. L. Yun,[2,3] A. Frasca,[4] A. C. Lanzafame,[4,5] J. E. Drew,[6] J. Eislöffel,[7] R. Blomme,[8] T. Morel,[9] A. Lobel,[8] T. Semaan,[9,10] S. Randich,[11] R. D. Jeffries,[12] G. Micela,[13] A. Vallenari,[14] V. Kalari,[15] G. Gilmore,[16] E. Flaccomio,[13] G. Carraro,[17] C. Lardo,[18] L. Monaco,[19] L. Prisinzano,[13] S. G. Sousa,[20] L. Morbidelli,[11] J. Lewis,[16] S. Koposov,[16] A. Hourihane,[16] C. Worley,[16] A. Casey,[16] E. Franciosini,[11] G. Sacco[11] and L Magrini[11]

Affiliations are listed at the end of the paper

Accepted 2016 May 18. Received 2016 May 18; in original form 2016 March 2

ABSTRACT

The young open cluster NGC3293 is included in the observing program of the *Gaia*-ESO survey (GES). The radial velocity values provided have been used to assign cluster membership probabilities by means of a single-variable parametric analysis. These membership probabilities are compared to the results of the photometric membership assignment of NGC3293, based on *UBVRI* photometry. The agreement of the photometric and kinematic member samples amounts to 65 per cent, and could increase to 70 per cent as suggested by the analysis of the differences between both samples. A number of photometric PMS candidate members of spectral type F are found, which are confirmed by the results from VPHAS photometry and SED fitting for the stars in common with VPHAS and GES data sets. Excesses at mid- and near-infrared wavelengths, and signs of Hα emission, are investigated for them. Marginal presence of Hα emission or infilling is detected for the candidate members. Several of them exhibit moderate signs of *U* excess and weak excesses at mid-IR wavelengths. We suggest that these features originate from accretion discs in their last stages of evolution.

Key words: stars: pre-main-sequence – open clusters and associations: general – open clusters and associations: individual: NGC 3293.

1 INTRODUCTION

Young open clusters (YOCs) are the best astronomical targets for obtaining physical information on the properties of forming stars, and for checking models for the initial phases of stellar evolution. The growing availability of large spectroscopic and photometric data sets has triggered several recent studies of young stellar populations in YOCs and associations (see, e.g. Chené et al. 2012; Spina et al. 2014; Cantat-Gaudin et al. 2014).

In this framework, the Stellar System Group (http://ssg.iaa.es) has produced catalogues of candidate members, based on photometric properties, in around 20 YOCs (see Delgado et al. 2013, and references therein). The procedure for member selection has been described and applied to a sample of 11 southern clusters by Delgado, Alfaro & Yun (2007, 2011; hereafter DAYI, DAYII). A spectroscopic assessment of this method for selecting photometric candidate members is now possible for NGC 3293, the only cluster in our sample which is also included in the observations of the *Gaia*-ESO Spectroscopic Survey (GES).

GES is an ambitious public spectroscopic survey that is obtaining medium- and high-resolution spectroscopy of some 100 000 stars in the Milky Way, including several fields towards YOCs (Gilmore et al. 2012). The observations started on December 31, 2011 and are carried out on the Very Large Telescope (VLT) at the Paranal Observatory, Chile. All the data collected by the Survey are homogeneously reduced and analysed by the *Gaia*-ESO consortium. Observations are conducted with the FLAMES (Fibre Large Array Multi-Element Spectrograph) multi-fibre facility (Pasquini et al. 2002). Medium resolution spectra ($R \approx 20\,000$) of about 10^5 stars are being obtained with Giraffe and high-resolution spectra ($R \approx 47\,000$) of about 5000 stars are being obtained with UVES (the Ultraviolet and Visual Echelle Spectrograph, Dekker et al. 2000).

One of the main GES objectives is to provide radial velocities (RV) with good precision for stars in YOCs, to complement *Gaia*

⋆ Based on data acquired by the *Gaia*-ESO survey programme ID 188.B-3002. Observations were made with ESO Telescopes at the La Silla Paranal Observatory.

† E-mail: delgado@iaa.es

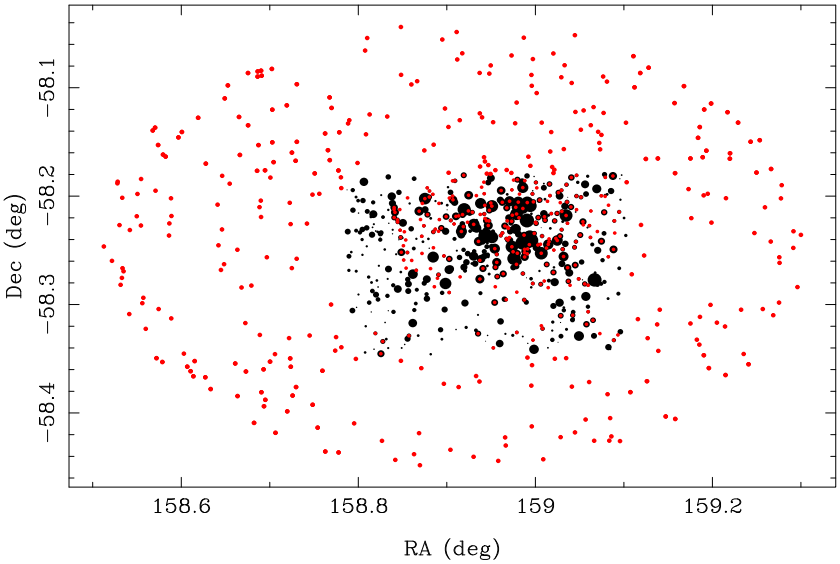

Figure 1. Schematic map of the field towards NGC 3293, showing all objects with GES observations as red dots, and the stars inside the DAYII FOV as filled black circles of brightness-coded size. Only stars with photometric detection in all UBVRI bands in DAYII are plotted for clarity.

proper motions with comparable accuracy for a statistically significant sample (Gilmore et al. 2012; Randich et al. 2013). A particular interest of the project is centred on the study of potential pre-main sequence (PMS) candidate members in some YOCs.

The cluster NGC 3293 is one of the targets of the GES project. It is located in the Carina-Sagittarius spiral arm of the Milky Way, and exhibits a tight concentration of bright stars that stand out against the field. This is actually reflected in a large number of main sequence (MS) candidate members of spectral type B in the colour–magnitude (CM) diagrams. The GES data in the cluster field provide an independent assessment of the quality of the photometric membership assignment, and also allows us to study the physical properties of PMS cluster members, with particular focus on PMS candidate members of spectral type F. In the next section we describe the data used in the study. In Section 3 we explain the methods of membership assignment and their results. Section 4 deals with the presence in the cluster of candidate PMS members of spectral type F. Their properties are discussed in Section 5, and Section 6 contains the main conclusions of the work.

2 DATA ON NGC 3293

The cluster NGC 3292 is located at RA = $10^{h}35^{m}48.77^{s}$, Dec = $-58^{\circ}13'28.1''$ (Epoch 2000). It has been the subject of several photometric studies (i.e. Feinstein & Marraco 1980; Turner et al. 1980, hereafter T80; Baume et al. 2003, DAYI, DAYII). The photometric observations by DAYI and DAYII include 1337 stars detected in at least the *BV* bands, with 490 of them detected in all five *UBVRI* bands. These are the data used in the present analysis. The values of the cluster parameters given by these authors amount to $E(B-V) = 0.29\pm0.04$, $DM = 12.0\pm0.2$, LogAge(yr) $= 6.8\pm0.07$. Matching with the 2MASS database (Skrutskie et al. 2006) provides heliocentric coordinates for all stars, and 2MASS identifiers together with near-infrared (NIR) colour indices for the stars in common. The photometric catalogue is included as online data in DAYII, and can also be accessed on the Stellar Systems Group website (http://ssg.iaa.es).

The *Gaia*-ESO consortium is structured into several working groups (WGs) that deal with all the relevant tasks, from target selection and observations, to data analysis and data archiving. Data reduction and RV determinations are performed by WG7 and WG8, respectively. The analysis of PMS stars is carried out by WG12 (Lanzafame et al. 2015) and the analysis of high-resolution UVES spectra for FGK type stars, more than 2000 to date, is carried out by WG11 (Smiljanic et al. 2014). The survey's analysis is performed in cycles, following the data reduction of newly observed spectra, with improvements of the various steps involved. At the end of each cycle an internal data release (iDR) is produced and made available within the *Gaia*-ESO consortium for scientific validation. In our case, we will use the RV and $T_{\rm eff}$ data of the iDR2+iDR3 release, provided by WG13, and placed in the GES archive at the Wide Field Astronomy Unit at Edinburgh University (`http://ges.roe.ac.uk/`).

The fields covered by the spectroscopic and photometric data sets are represented in Fig. 1. The GES data include 536 stars in the field of NGC 3293, selected primarily on the basis of available photometry, both optical and infrared. Additional considerations finally led to the explicit inclusion of probable field stars so as to cope with all the objectives of the GES project. Only stars detected in all five *UBVRI* bands are represented in the optical field of view (FOV). The gaps observed in its southern half could be caused by an actual lack of detections due to obscuring clouds that surround the cluster. The total selected sample is distributed almost in equal numbers between stars with high probability of cluster membership, and probable field stars. Only eight stars among the 536 in the sample were observed with UVES, U520. The FLAMES–Giraffe setups quoted in the released data for targets in the field of this cluster are HR3, HR5A, HR6 and HR9B for most stars. They cover the spectral range 4033–5356 Å, and resolutions in the MEDUSA mode around $R = 20\,000$. Of these 536 stars, 530 have RV values between -100 and $+100$ kms^{-1}. This is the star sample that we consider in our kinematic membership analysis, and they are plotted as red dots in Fig. 1. Among them, 232 have RV errors listed in the used GES data release, with 75 located inside the photometric FOV. The median of their errors amounts to 0.4 km s^{-1}, a value similar to those reported by other authors for GES RV data (e.g. Jeffries et al. 2014; Guiglion et al. 2015; Rigliaco et al. 2016). Jackson et al. (2015) compiled 8500 stars in eight clusters observed by GES, and analysed the variation of the RV uncertainty as a function of S/N

ratio, $v\sin i$, and stellar properties. Their fig. 1 shows the distribution of the empirical RV uncertainty versus the S/N ratio for different intervals of $v\sin i$. These plots offer a clarifying vision of how the GES empirical RV uncertainty behaves for different parameters and of what we can expect for our data.

3 MEMBERSHIP ASSIGNMENTS

In clusters of ages around 10 Myr, PMS stars up to spectral type F are expected. They would be in advanced evolutionary stages, showing reduced signs of PMS nature, such as accretion disc, emission features, and near- or mid-infrared excess, as compared to younger and later type PMS stars (Sicilia-Aguilar et al. 2005; Luhman & Mamajek 2012; Delgado et al. 2013). This would make them relatively more difficult to detect (de Winter 1997). Their search and assignment, however, is of obvious importance for a proper determination of the mass distribution of the cluster, and our photometric membership assignment procedure is aimed at the detection and study of PMS stars in YOCs of the mentioned age.

3.1 Photometric membership

The photometric members are selected according to the procedure discussed in DAYI, based on *UBVRI* CCD photometry. Possible main sequence and evolved stars are selected visually in each photometric diagram, as illustrated in the upper panel row of Fig. 2. In the lower panel row, stars selected in at least one of the five diagrams are marked as larger dots, and those selected in all five diagrams simultaneously are marked in red. The latter constitute the initial sample of B-type MS, and evolved members.

Colour excess values are measured in the $(U-B)$, $(B-V)$ colour–colour diagram, also obtaining absolute magnitudes M_V and distance modulus values, $DM = V - R{*}E(B-V) - M_V$. Here we use values for the reddening slope and absorption coefficient $\alpha = E(B-V)/E(U-B) = 0.74$ and $R = 3.1$, as given by T80. The diagram $V - 3.1 \times E(B-V)$, M_V (Fig. 3) is used in combination with all four CM diagrams to refine the selection. Unevolved B-type MS members (blue dots), which define the colour excess and the distance modulus of the cluster, are separated from evolved members (magenta dots), used in the calculation of cluster age by quantitative comparison with post-MS isochrones. Stars plotted as green dots occupy consistent locations in all photometric diagrams, and are not excluded as members, but are not considered for the calculation of the cluster parameters.

For all the remaining stars, colour excess and M_V values are calculated in the CC diagram with respect to the ZAMS and PMS isochrones, whereby we assume that the $(U-B)$, $(B-V)$ relation for the PMS isochrones is the same as for the ZAMS (Siess, Dufour & Forestini 2000). The calculated colour excesses and distance moduli are compared with the average value of the unevolved MS B-type candidates.

The procedure is also applied to stars without valid U measurement. This is frequently the case for potential cluster members in the faintest part of the CM diagrams. Neither colour excess nor distance values can be calculated for them in the CC diagram. We then assume that they have a colour excess equal to the median value of the candidate members with U measurement, and measure the distance to PMS isochrones in the three remaining CM diagrams. Membership is assigned in a CM diagram when the measured distance coincides within errors with the average value for selected B-type MS unevolved candidate members. The assignment also produces values of mass, luminosity and effective temperature for

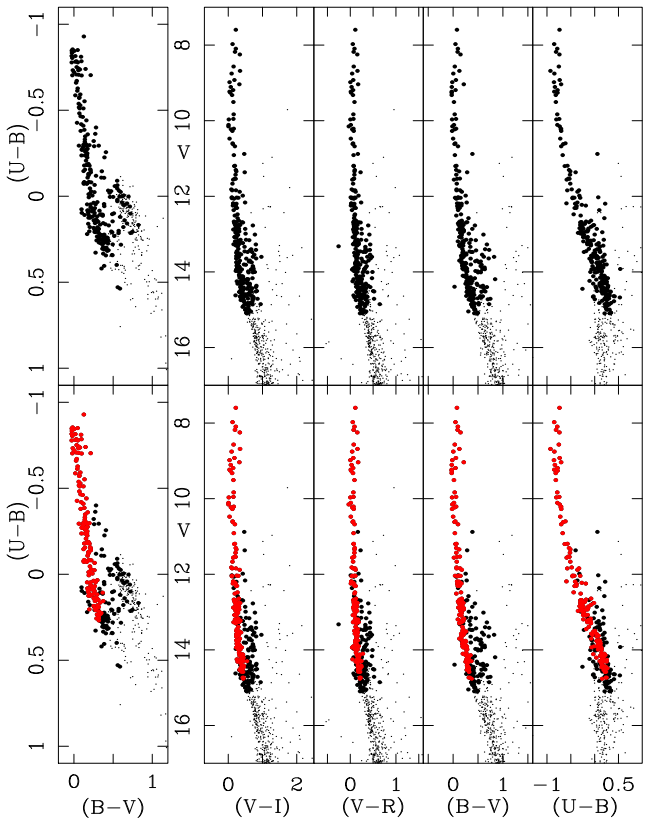

Figure 2. Plots of the $(U-B)$, $(B-V)$ CC diagram, and the four CM diagrams, V versus colour indices $(V-I)$, $(V-R)$, $(B-V)$ and $(U-B)$, in five panels from left to right. In the upper row, larger dots represent possible stars defining the expected main sequence and evolved stars in each diagram. In the lower row, larger dots represent stars selected in this way in at least one of the five diagrams, while red dots represent those stars selected in all five diagrams simultaneously.

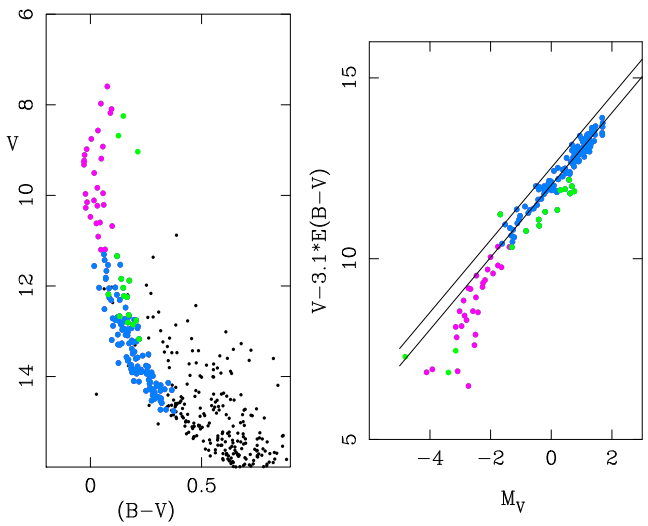

Figure 3. In the right-hand panel the quantity $V - 3.1 \times E(B-V)$ is plotted versus M_V. Lines correspond to maximum (upper line) and average distance modulus of the B-type unevolved MS members, indicated with blue dots. Magenta dots represent evolved stars, used to calculate cluster age. Joint inspection with the CM diagrams, such as the V,$(B-V)$ diagram shown in the left-hand panel, leads to excluding the candidate member stars plotted as green points from these two samples (see the text, Section 3.1).

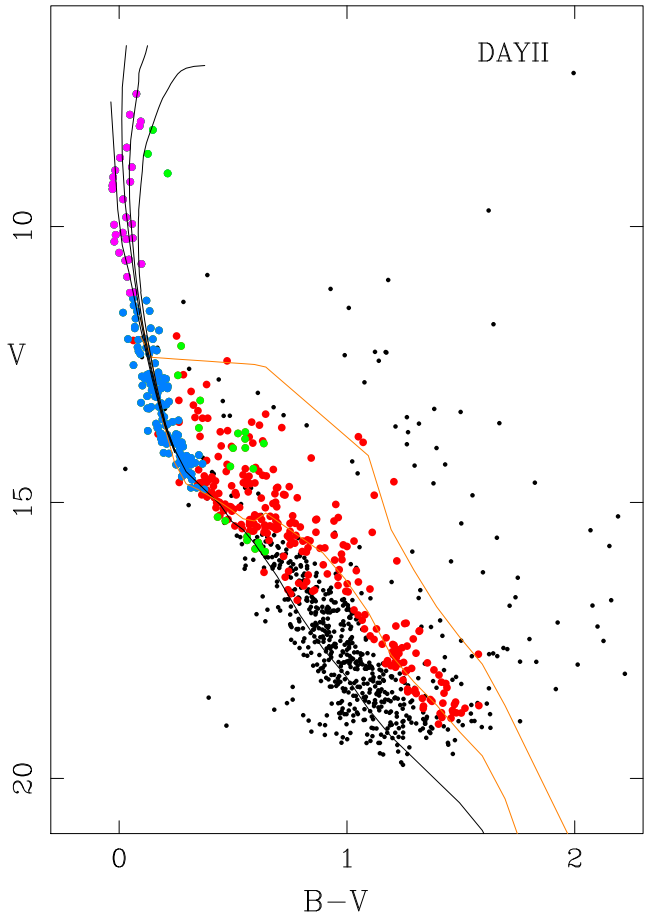

Figure 4. CM diagram V, $(B-V)$ of NGC 3293, showing the photometry by DAYII. The photometric candidate members used to calculate cluster reddening, distance and age are the MS candidate members (blue dots), and post-MS members as magenta dots. PMS candidates are plotted as red dots. Green dots represent stars kept as MS and post-MS candidate members, not used to calculate the cluster parameters. The ZAMS and post-MS isochrones for LogAge(yr) = 6.6, 7.0, 7.4 are plotted as black lines. PMS isochrones of ages 1 and 10 Myr are plotted as orange lines. All of them are shifted to account for the mean $E(B-V)$ and DM of the unevolved B-type MS candidate members (see Fig. 3), $E(B-V) = 0.29$, DM = 12.02.

the candidate member. Stars selected as members in at least three CM diagrams, and with photometric errors in all indices below 0.05 mag constitute the finally selected member sample.

We draw attention to a group of stars with $(B-V)$ values in the range $0.5 < (B-V) < 1.0$, which would correspond to reddened F-type stars, but exhibit abnormally blue values on the $(U-B)$ index. Their shifting in the CC diagram leads to colour excesses and M_V values indicative of highly reddened B-type background stars. However, many of them turn out to be assigned as F-type PMS members, if we assume them to be affected by the median $E(B-V)$ cluster value, and calculate a distance for them in the way described above for stars without U detection. We ask whether some of these stars would be part of a background population, or if they are actual F-type PMS cluster members with a peculiar excess on the $(U-B)$ colour index. We name these stars UF stars for brevity, and will come back to them in Section 4 below.

The total number of selected candidate members amounts to 439 stars, with 189 and 250 stars respectively as MS and PMS candidate members. They are indicated in Fig. 4, where we plot the CM diagram V, $(B-V)$, with indication of the photometric member samples

3.2 Kinematic membership

The RV values produced by the GES observations have been used to estimate cluster membership probabilities. We consider that the RV distribution of the sample can be modelled by the sum of two 1D Gaussians corresponding to the cluster and field populations respectively (Vasilevskis, Klemola & Preston 1958; Geller, Latham & Mathieu 2015; Sampedro & Alfaro 2016). The RV probability density function for the sample stars can then be written as:

$$\Phi(RV) = n_c \Phi_c(RV, RV_c, \sigma_c) + (1-n_c)\Phi_f(RV, RV_f, \sigma_f) \quad (1)$$

where $\Phi_c(RV)$ and $\Phi_f(RV)$ are two 1D Gaussians with mean RV_c and RV_f, and standard deviations, σ_c and σ_f, which correspond to the cluster and field kinematic populations respectively, and where n_c is the fraction of cluster stars in the sample. According to *Bayes* theorem the probability of one star with RV being a cluster member is given by the expression:

$$P_c(RV) = \frac{n_c \Phi_c(RV, RV_c, \sigma_c)}{n_c \Phi_c(RV, RV_c, \sigma_c) + (1-n_c)\Phi_f(RV, RV_f, \sigma_f)}. \quad (2)$$

The model depends on five parameters and their estimation, and subsequent classification of the stars into both groups can be done simultaneously following the method proposed by Cabrera-Caño & Alfaro (1985) for the case of proper motion distribution (2D), easily tied to the case of one dimension. The previous purge of the sample of possible outliers is necessary, as pointed out by Zhao et al. (1982). The very concept of 'outlier' belongs to the rare family of mathematical objects not rigorously defined. The outlier nature of a given object can only be presumed, especially if the only information on the parent distribution is the sample at hand. In order to estimate the probability of a sample star being an outlier we used the OUTKER method (Cabrera-Caño & Alfaro 1985), and as the outlier selection criterion we adopted the *Bayes* minimum error rate decision rule: i.e. we consider any star to be an outlier if it has a probability larger than 0.5 of being so. A total of 28 stars were classified as outliers and removed from the initial sample of 530 stars (Fig. 5).

The membership assignment is performed with the aforementioned methodology. As illustrated in Fig. 5, this method estimates the membership probabilities by fitting the RV distribution with two Gaussians, one for field stars and another for cluster members. Starting with reasonable values for the distribution's parameters, membership probabilities are then estimated using the *Bayes* theorem. Through an iterative Wolfe estimation procedure (Wolfe 1970), a new determination of the parameters is carried out. Membership probabilities are recomputed and used again to estimate new parameters until convergence is reached, providing a membership probability for every star. After imposing a minimum probability threshold of 50 per cent (adopting the *Bayes* minimum error rate decision rule), we end up with 216 kinematic probable members in the total GES sample. Given the probabilistic character of the problem, a non-null misclassification rate is expected. On the basis of the distribution of probabilities obtained, this would amount to an estimated 15 per cent of the total sample. The parameters of our 1-D two-Gaussians model are: $\mu_c = -11.5$, $\sigma_c = 3.7$, and $\mu_f = 4.1$, $\sigma_f = 20.3$ km s^{-1}. The precision of RV single measurements is around 0.4 km s^{-1} (Jackson et al. 2015), but the value of σ_c is one order of magnitude higher, and dominated by actual RV uncertainties, which would originate in the presence of a populated

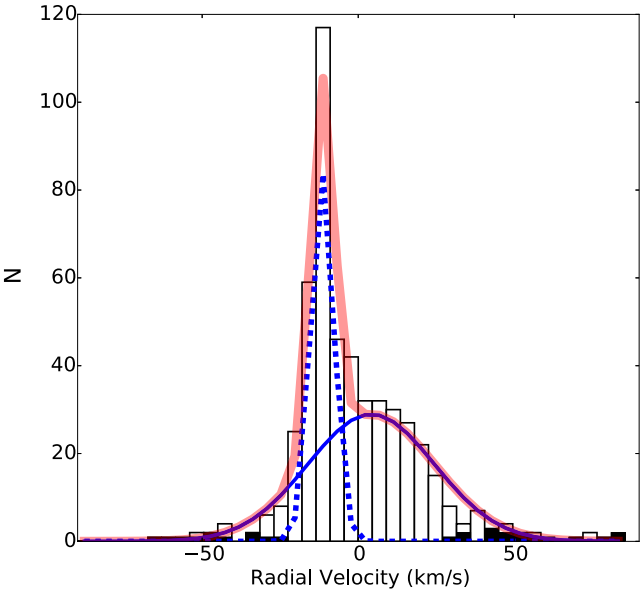

Figure 5. Radial velocity (RV) distribution for the 530 stars in the GES data included in our analysis (empty histogram). The filled histogram represents the 28 stars excluded as outliers (see the text). The RV distribution is reproduced by the fit of two Gaussian functions: one for field stars (solid blue line) and another for cluster members (dashed blue line), whose sum is overplotted as a solid red line.

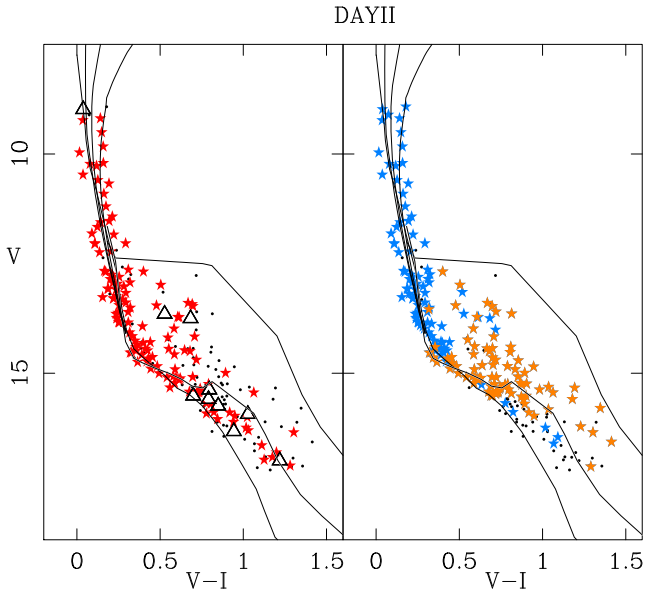

Figure 6. Distribution in the CM diagram V, $(V-I)$ of stars with and without kinematic membership assignments, and comparison to their selection as photometric candidate members. In both panels, stars with GES data in the optical FOV are plotted. The left-hand panel shows as red stars those selected as kinematic members, and as black triangles those rejected as outliers. The right-hand panel shows those among them selected as photometric MS+post-MS, and PMS members, marked respectively in blue and orange colours. The ZAMS and isochrones are plotted as in Fig. 4.

distribution of binary and/or multiple stellar systems, commonly found in YOCs harbouring many massive stars (Cottaar & Hénault-Brunet 2014). This implies that the consideration of the individual precision errors would not have an influence on the results of our pdf model fitting, and the assignment of probable members. A careful analysis of the cluster dynamics (e.g. Cottaar & Hénault-Brunet 2014) lies outside the scope of this paper.

3.3 Membership comparison

The total samples of 530 and 1337 stars, in the spectroscopic and photometric data by GES and DAYII respectively, have 227 stars in common, with 217 among them not rejected as outliers (Section 3.2). Among these 217 stars, 128 and 171 stars are assigned as kinematic and photometric members respectively, with 111 objects in common.

We refer in the following to this common sample of 227 stars, for which both membership assignments can be studied and compared to each other. In Fig. 6 we compare the respective distributions of kinematic (left-hand panel) and photometric members (right-hand panel) in the CM diagram. This comparison presents interesting features. We note that five stars kinematically marked as outliers are photometrically selected as members, in particular three of them among the MS and post-MS members. This illustrates the nature and comparative achievements of both membership assignment procedures. The photometric membership assignment is entirely based on the physical properties of the stars, as given by models of different types, and on their expected properties according to these models. The kinematic probability is otherwise based on an assumed kinematical structure, such as a Gaussian distribution, and furthermore relies on the particular distribution of the one parametric projection represented by the RV value. One could summarize the different approaches by stating that the key words, and also those affected by the basic uncertainties in either method, are 'probable' in the kinematic procedure, and 'member' in the photometric one. The models, assumptions and results are therefore of a different nature, and in particular the kinematic definition of members, non-members and outliers might mix, exclude or include stars with a good quality as photometric members. On the other hand, the quality of the photometric membership is obviously affected by uncertainties. We also observe that the largest discrepancy of photometric candidate members not assigned as probable kinematic members are among the PMS photometric candidates: 60 per cent of the PMS candidates are kinematically selected, whereas the percentage rises to 81 per cent among the MS and post-MS photometric candidates. We discuss possible causes for the discrepancies between both membership assignments in each sense.

3.3.1 Photometric candidate members with deviating RV value

Among the 171 photometric candidate members (Section 3.3), 60 stars are not selected by the kinematic analysis. This discrepancy can be partly explained if we consider that *RV* values could indeed change between epochs, and between studies due for instance to the presence of undetected binary companions in some stars (Geller et al. 2010).

The results by Dufton et al. (2006; hereafter D06) are an example of this. They give *RV* values for 29 stars in the field of NGC 3293 in common with our GES data. All of them are among our photometric candidate members, with 24 of them also selected as kinematic members. However, nine of these stars, of which five are among our kinematic members, have RV values by D06 that differ from GES values by more than 40 kms^{-1}. This comparison shows that part of the photometric candidates not selected by the kinematic assignment could be caused by actual variations in the RV value.

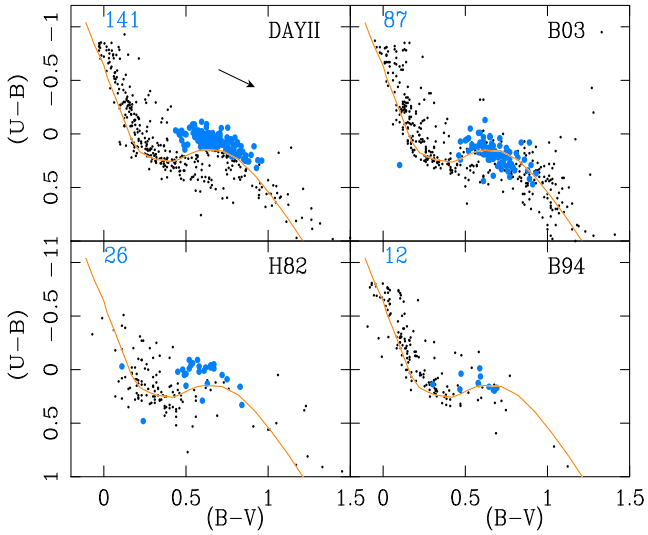

Figure 7. $(U-B)$, $(B-V)$ diagram by DAYII, B03, H82 and B94. The orange line represents the ZAMS, shifted by values $E(B-V)=0.22$, $E(U-B)/E(B-V)=0.74$. An arrow shows the direction and length of the reddening vector in the upper left panel. Blue points denote the UF stars in common. Their respective numbers are quoted in each panel.

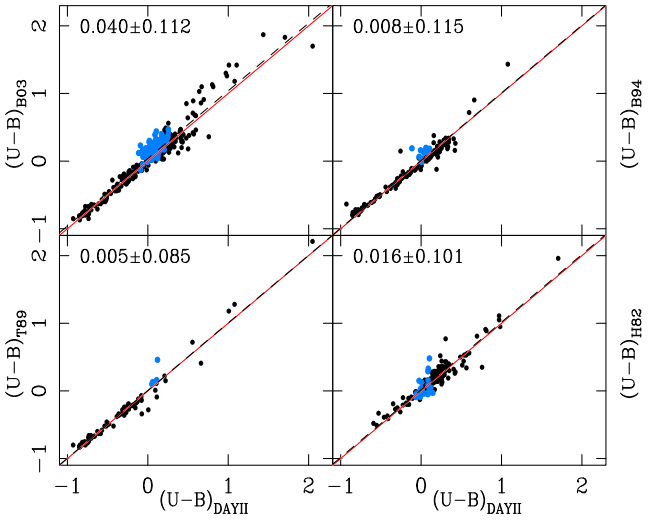

Figure 8. Differences between $(U-B)$ values of B03, B94, T80, and H82 and DAYII. In all panels, a red line represents the slope 1, and a black line the average difference between the corresponding $(U-B)$ values and those by DAYII. The average values of the differences and their rms are quoted.The so-called UF stars are marked in blue.

We come back to this discrepancy in the discussion of the UF stars mentioned above (Section 3.1)

3.3.2 Kinematic candidate members without photometric assignment

Of the 128 kinematic candidate members (Section 3.3), 17 stars are not selected as photometric candidates. These are stars with an RV value very close to the systemic velocity of the cluster, but rejected from any photometric membership. They are most probably non-cluster members. A simple estimate can be made considering the distribution of RV for the field as represented by the RV values of GES targets located outside the photometric FOV (see Fig. 1). From this we estimate an approximate number of 14 field stars that would still be at their present locations and with their RV values also in absence of any cluster. The 17 stars referred to above would indeed be representative of this contaminating group. This would mean a field contamination of 13 per cent of the total kinematic members sample (17/128) in the photometric FOV, a value similar to the estimated misclassification rate for the whole sample (Section 3.2).

4 PMS CANDIDATE MEMBERS OF SPECTRAL TYPE F

In the photometric membership assignment, a number of stars are found that exhibit abnormally high values of the $(U-B)$ index (Section 3.1). They are just selected visually in the DAYII $(U-B)$, $(B-V)$ diagram, and are plotted as blue dots in Fig. 7, where this CC diagram is shown for DAYII photometry, and for available photometric results with stars in common. These are *UBVRI* CCD photometry by Baume et al. (2003, hereafter B03 in the following), *uvby*Hβ CCD photometry by Balona (1994, hereafter B94), photoelectric *UBV* photometry by T80, and photographic *UBV* photometry by Herbst & Miller (1982, hereafter H82). The *uvby* photometric indices of B94 are transformed to *UBV* indices with calibrations by Harmanec & Bozic (2001, hereafter HB01), which are elaborated with the *uvby* catalogue compiled by Hauck & Mermilliod (1998). The CC relation plotted in Fig. 7 is the ZAMS line. We note that the PMS isochrone sets used to estimate PMS membership consider the same $(U-B)$, $(B-V)$ relation for PMS and MS stars. Recent studies of the PMS isochrones (Bell et al. 2014), and PMS colour–$T_{\rm eff}$, colour–BC relations (Pecaut & Mamajek 2013) do not include the $(U-B)$ index in their results. In a previous study (Delgado et al. 1998) it was found that the $(U-B)$,$(B-V)$ relation for class III and later stars was acceptably similar to the one used for dwarfs. In any case, the possible luminosity effects on the $(U-B)$ colours of PMS candidates are expected to reflect in comparatively redder, rather than bluer colours, for stars of lower gravity than their MS counterparts.

These stars show some puzzling properties that we shall discuss in some detail. The differences between $(U-B)$ values in DAYII and these photometric studies are plotted in Fig. 8. These are small although with high dispersion. The photometry by B03 presents the highest value. As can be seen in the plot, the differences for $(U-B)$ < 0 are also smaller, with lower dispersion. For B03 they amount to 0.009 ± 0.053. This rms value will be used as limiting difference to define coinciding values in the discussions below.

The differences in the interval $-0.1 < (U-B) < 0.3$, where the UF stars are found, are shown in Fig. 9. In each panel the average differences from Fig. 8 are quoted, compared to those calculated for only the UF stars in common in the respective photometries. Several facts stand out from these differences. On the one hand, the redder value for the UF stars in three photometries would lead to suspect that some systematics is present in the $(U-B)$ calibration by DAYII. On the other hand, only B03 among these three sets has a considerable number of UF star in common with DAYII, and we also observe that the H82 values exhibit agreement with DAYII, although with a high dispersion. Furthermore, there are common stars between DAYII and all photometries, which exhibit quite coincident values as defined above, with B03 photometry in particular. We indeed observe a collection of stars, mainly in B03 and H82 photometries, which have coincident values with DAYII, and simultaneously exhibit comparatively bluer $(U-B)$ values as

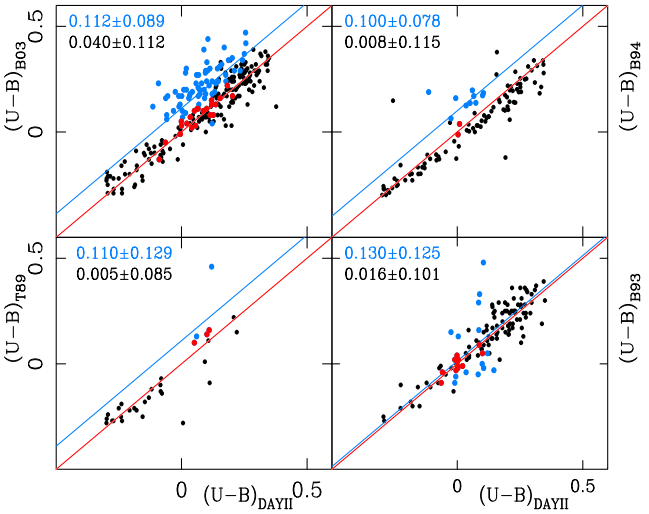

Figure 9. Differences between $(U-B)$ values of B03, B94, T80, and H82 and DAYII for $-0.1 < (U-B) < 0.3$. The average values of the differences and their rms are quoted in black for differences in the whole respective $(U-B)$ ranges in common, and in blue figures for the differences between the values of common UF stars. Red dots mark the UF stars with coinciding values in each photometry, and also in common with GES.

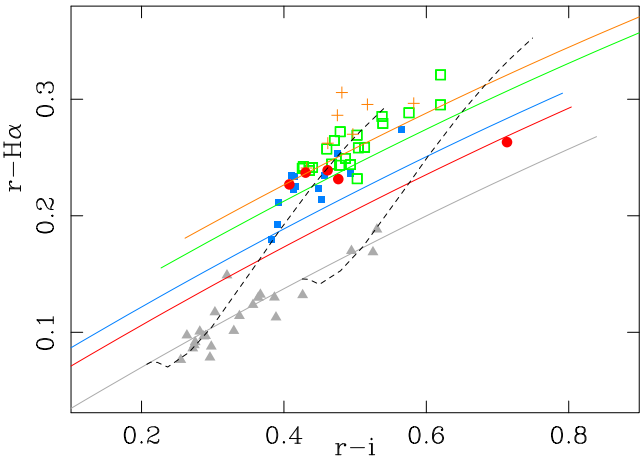

Figure 10. Diagram $(r-\mathrm{H}\alpha)$,$(r-i)$ from the VPHAS+ database, for stars in common with DAYII and GES. Grey triangles mark selected A type stars. UF stars are plotted as red filled circles, blue filled squares, green open squares and orange crosses, corresponding to the spectral ranges F0, F0−F2, F2−F5, and F5−F8, respectively. Lines of corresponding colours represent, from bottom to top, the reddening lines for spectral types A0, F0, F2, F5 and F8. Broken ascending lines represent the ZAMS for absorption values $A_V = 1$ (left) and $A_V = 2$ (right).

plotted in Fig. 7. Those among them in common with GES are marked as red symbols in all panels.

The combination of all the properties of the UF stars shown in the plots above actually moves to a deeper analysis of these stars with the data sets available. We will now describe the results of Spectral Energy Distribution (SED) fitting, based on $T_{\rm eff}$ values from GES, and the analysis of the *ri*Hα photometry for the UF stars in common with the VPHAS+ database (Drew et al. 2014).

4.1 UV excess originated in accretion discs

Continuum excess luminosity, which is best detected at wavelengths shorter than the Balmer jump, is a primary indicator of accretion on to a PMS star (e.g. Alcalá et al. 2014, and references therein). It has been suggested that the effects of accretion from discs show in ultraviolet (UV) excess in PMS stars of the T-Tauri type in the cluster NGC 2264 (Rebull et al. 2002), and the results by DAYII on the basis of photometry agree with these results.

The possible presence of accretion discs in F-type PMS stars has been studied by Suchkov, Schultz & Lisse (2002; hereafter S02). They find a number of candidates with discs, which they associate with the continuation to redder spectral types of the HAeBe stars. They also propose a considerable increase in the number of known F-type PMS stars, in a $T_{\rm eff}$ range covered by our UF stars.

4.1.1 Possible Hα emission

If some of the UF stars are indeed accretors, it is likely they would be associated with some Hα line emission. This possibility has been tested using bandmerges of the Hα and *r*, *i* photometry available from the VST Photometric Hα Survey of the Southern Galactic Plane and Bulge (VPHAS+, described by Drew et al. 2014). Fig. 10 shows the $r-\mathrm{H}\alpha$, r − i plot obtained for UF stars and a set of spectroscopically confirmed early A stars in common with this database.

In this diagram, an object with Hα emission superposed on its normal photospheric spectrum will appear displaced upwards relative to the reddening line appropriate to its spectral type (Kalari et al. 2015; see Drew et al. 2014 for tables of reddening lines). As would be expected for a selection of normal field A stars, there is no noticeable $(r-\mathrm{H}\alpha)$ excess, except in one object. The average value of the calculated excesses for the individual stars amounts to $\Delta(r-\mathrm{H}\alpha) = -0.001 \pm 0.015$.

The situation is somewhat different for the UF stars. Fig. 10 provides reddening lines for F0, F2, F5 and F8 photospheric spectra, chosen to match the range in subtype among the UF stars: compared to the appropriate reddening line, they are displaced upwards in $(r-\mathrm{H}\alpha)$, occupying the range $0.0 < \Delta(r-\mathrm{H}\alpha) < 0.05$. The specific calculation of their excesses gives the average value $\Delta(r-\mathrm{H}\alpha) = 0.019 \pm 0.021$. In view of the ∼100 Å FWHM of the VST Hα filter, these excesses map on to implied Hα emission equivalent widths of 0–5 Å, with no apparent trend with the calculated excesses in the *U* and infrared bands (Section 4.1.2 below). We remark that the diagram can also be read for evidence favouring extinctions for the UF stars of $A_V \geq 1$, (or $E(B-V) \geq 0.32$, for an $R = 3.1$ law). It is important to note that the probable error in the individual excess measurements (0.02–0.03) is a significant fraction of the mean excess, indicating that no one measurement in isolation is of high significance. In short, the group of objects as a whole is consistent with the presence of at most marginal infilling or self-reversing Hα emission.

4.1.2 Analysis of UF stars with SED fitting

The possibility of excesses in various wavelength ranges has been further checked by means of SED fitting to the *BVRIJH* data of the UF stars. The *JHK* magnitudes have been obtained from 2MASS for the stars in common (Skrutskie et al. 2006). We fitted the observed SEDs with photosphere model spectra as done by Frasca et al. (2015) for the members of γ Vel and Cha I clusters. In brief, we adopted the grid of NextGen synthetic spectra, with $\log g$ in the range 3.5–5.0, $T_{\rm eff}$ from 1700 to 10 000 K, and solar metallicity by Hauschildt, Allard & Baron (1999) from which we derived the surface fluxes in the *BVRIJH* passbands that were interpolated to the stellar temperatures and gravities. We adopted the

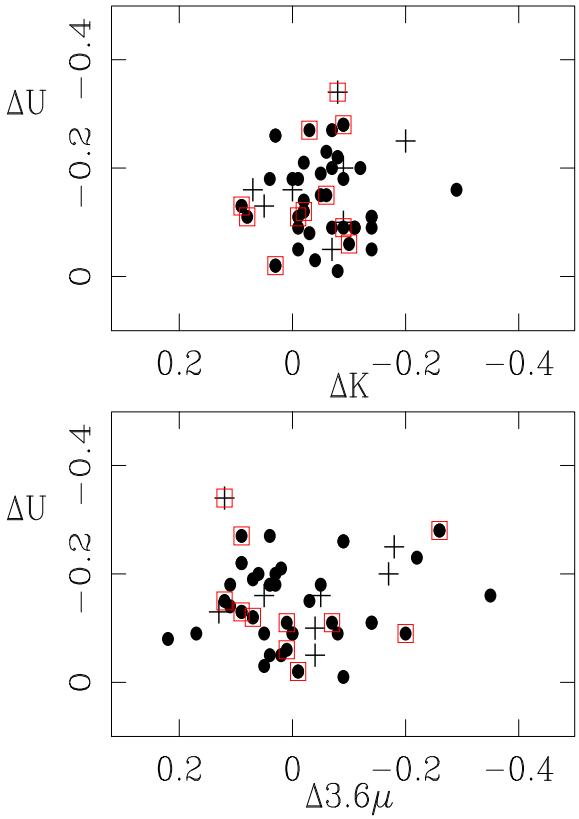

Figure 11. Plots of the U excesses by SED fitting, versus excesses in the near- and mid-infrared bands, K and IRAC 3.6μ bands, respectively. Dots and crosses represent candidate members and non-members respectively, considering both kinematic and photometric criteria together. Red squares mark the stars with coinciding $(U-B)$ values in other photometries (Section 4).

GES values of $T_{\rm eff}$ and $\log g$ and fixed the cluster distance to 2.5 kpc (DAYII), leaving the stellar radius and the extinction, A_V, free to vary until the minimum of χ^2 was reached. We find that the extinction values are in the range found for the cluster members by DAYII. This supports the cluster membership of these stars as F-type PMS members.

The Vela–Carina catalogue of Spitzer point sources (Churchwell et al. 2009) contains 684 stars in common with our photometry. According to the YSO classification schemes for IRAC photometry by Allen et al. (2004) and Gutermuth et al. (2009), no sources in this sample occupy the regions in the ([3.6]–[4.5])/([5.8]–[8.0]) diagram typical of Class I or Class II sources. Concerning the UF stars, the above referred SED fits produces values of the excesses in U-band and K, and IRAC bands. The U-band excesses are in the same range as those that come from the photometry. In Fig. 11 we have plotted these U excess values versus those obtained at the K and IRAC 3.6μ bands.

The figure shows low IR excesses, with relatively higher values for some UF stars at mid-IR wavelengths. The values of the U excess obtained are to be compared to those for PMS stars of later spectral types in the YOC NGC 2264, given by Rebull et al. (2002). In a similar range of EWHα values (0–5 Å), U excess values in TTau type stars are a factor of 3 larger than those calculated for our F-type PMS candidates. These features agree with the proposed decrease of the time-scale of disc dissipation with both increasing age and star mass (Pecaut, Mamajek & Bubar 2012; Hernandez et al. 2005; Hillenbrand 2008).

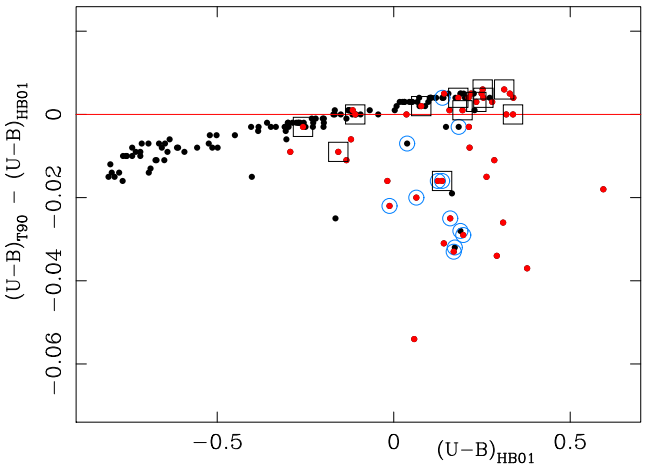

Figure 12. Comparison between $(U-B)$ indices obtained from B94 *uvby* photometry by calculation with the formulas by T90 and HB01. A red line marks the zero difference. The UF stars in common between DAYII and B94 are marked with blue circles. Photometric and kinematic PMS probable members are marked respectively with red dots and black squares.

5 DISCUSSION

The UF stars are immediately discarded as background highly reddened B-type stars by the $T_{\rm eff}$ values provided by GES. At least for the 52 of them in common with GES, effective temperatures between 6700and 7500 K are found, which correspond to spectral types later than A8 (Pecaut & Mamajek 2013). The effect of low metallicity is also discarded as the cause for some $(U-B)$ excess, at least for stars with available metallicity values. Models by Marigo et al. (2008) predict a variation in $(U-B)$ with metallicity at $(B-V)=0.6$ of 0.15 mag per dex, in good agreement with the results obtained by Cameron (1985). According to this, the excess in $(U-B)$ guessed for some of the UF stars would imply a metallicity around [Fe/H] $=-1.0$ for them. This is not supported by any of the metallicity values available for GES stars. The average value of metallicity for values given by GES amounts to [Fe/H] $=0.04\pm0.27$. For those stars also selected as kinematic members the average value amounts to [Fe/H] $=0.01\pm0.26$. Only four UF stars have GES metallicity values, which amount to [Fe/H] of 0.39, −0.21, 0.32, and 0.03. The same conclusion is reached from the metallicity values obtained for UF stars with *ubvy* photometry (B94). The [Fe/H] values derived from *uvby* photometry and the calibrations by Crawford (1975) and Schuster & Nissen (1989) are all greater than zero.

The comparison to other photometries opens the question of the possible systematics effects in the DAYII photometry. But we also see in these comparisons (Figs 7– 9), many stars in the same colour interval, several of them among the UF stars, which indeed have coinciding values in the various photometric studies. Furthermore, the comparatively redder $(U-B)$ values in B03 would actually be in part reflecting a slight but clear trend, appreciated in B03 photometry when compared to T80, B94 and H82.

An indication of the peculiarity of the named UF stars, independent of DAYII photometry, is shown in Fig. 12. In addition to the *uvby* to *UBV* calibration by HB01, we consider the one by Turner (1980, T90), claimed to be valid for $(U-B)<2$. In Fig. 12 we

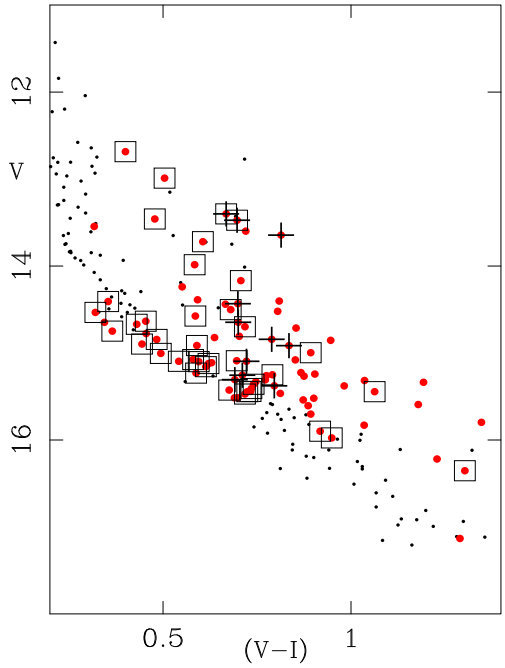

Figure 13. V,$(V-I)$ CM diagram for stars in common in DAYII and GES. Stars in common between DAYII and GES are plotted. Red dots are photometric PMS candidates, black squares those among them selected as probable kinematic members, and crosses mark the deviating stars observed in the plot of Fig. 12 (see the text).

plot the difference $(U-B)_{T90} - (U-B)_{HB01}$ versus $(U-B)_{HB01}$ for all the stars in the B94 *uvby* photometry. A trend of a few hundredths of magnitude is observed, as we move from blue to red colours, but the most prominent feature is the presence of several stars which detach towards comparatively bluer values in the T90 calibration. Interestingly enough, these deviating stars have two properties. First, all but one of the UF stars in common with B94 are among them. Secondly, most of them have photometric PMS membership assignment, marked as red points, while very few of them are also selected as probable kinematic members, marked as black squares. Such an exclusion amounts to only 18 per cent of the photometric members being also selected as probable kinematic ones (2 out of 11 with GES spectra), while among the photometric PMS candidates that follow the main trend observed in the plot this percentage increases to 77 per cent. We note that these deviating stars are part of the group of PMS photometric candidates not assigned as probable kinematic members mentioned in Section 3.3.

In Fig. 13 we plot a zoom of the CM diagram shown in Fig. 6, where only the photometric PMS candidates are plotted as red dots. Black squares represent those stars also assigned as probable kinematic members, while the deviating stars commented above are marked with crosses. We see that the PMS photometric members excluded from the kinematic assignment are preferentially located at comparatively redder colours and/or V values brighter than the ZAMS. This supports the suggestion of binarity being the origin of a variable RV, which causes the rejection of some of them as kinematic members, although they would actually be cluster members, and are indeed selected as such by the photometric procedure.

To summarize, the UF stars are visually selected because of their position above the ZAMS in the $(U-B)$,$(B-V)$ CC diagram by DAYII. A mixture of factors is certainly at the origin of this feature, with calibration errors, or background highly reddened field stars, among them. But the comparison to other photometries, and the results for those stars in common with the GES and VPHAS+ databases, demonstrates that many of them are best PMS cluster candidate members of spectral type F. Their properties show a practically negligible amount of Hα emission or even infilling, although the presence of accretion activity manifested in U excess is observed, which might reflect the presence of accretion discs in their last stages of evolution. The suggested discs could be at some intermediate stage between accretion discs and debris discs, and would be associated with the so-called weak-excess, pre-transitional or transitional discs (Espaillat et al. 2014). Most observational techniques for studying these discs are applied to stars at distances not farther than a few hundred parsecs and of spectral types K-M (Kim et al. 2013; Espaillat et al. 2014). We suggest that continuum observations with good precision and spatial resolution at far-IR (Moór et al. 2011) and, possibly, at sub-mm wavelengths (Isella et al. 2007; Carmona et al. 2014) could be used to detect possible dust emission from F-type PMS candidates (Andrews et al. 2013). However, the actual presence of U excess would be best checked with a homogeneous calibration of U photometry for F-type PMS candidates in clusters of ages, between 5 and say, 10 Myr. This should reduce the effects of systematic uncertainties. In addition to that, spectroscopic observations in a wavelength range covering the Balmer jump (Herczeg & Hillenbrand 2008) should provide confirmation of the presence or absence of a real U excess, which is commonly accepted as indicating accretion. Two stars among our F-type PMS candidate members, 2MASS10352172-5813111, and 2MASS10355556-5813117, both with kinematic and photometric membership assignment, would be appropriate targets. They are those marked with red squares and filled circles in Fig. 11, and U excess value above -0.2 mag.

6 CONCLUSIONS

(i) The GES release includes 536 stars in the field of NGC 3293, with 227 of them located inside the photometric FOV. In this sample, 171 stars are assigned as photometric members, and 128 as kinematic members, with the use of the GES RV values. A total of 111 stars have both membership assignments. This coincidence would improves when considering the presence of actual cluster members with variable RV, and the exclusion of contaminating field stars in the kinematic assignment methodology.

(ii) A sample of PMS candidate members of spectral type F is found in the cluster. Their proposed membership is supported by the comparison to previously published photometries, and the results of the analysis with SED fitting and the properties of their *ri* photometry, for the stars in common with GES and VPHAS+ databases.

(iii) The possible presence of Hα emission is studied on the basis of the $(r-\mathrm{H}\alpha)$ index from the VPHAS+ database. The calculation of excesses $\Delta(r-\mathrm{H}\alpha)$ indicates that the presence of Hα emission would only be marginal in the 43 UF stars in common with the VPHAS+ database.

(iv) The amount of U and IR excess in the UF stars is calculated by means of SED fitting of models with $T_{\rm eff}$ values provided by GES. IR excesses are calculated with the use of the 2MASS and IRAC bands. Little correlation between the U and IR excesses is found. Some continuum excess is however measured at mid-IR wavelengths for a few UF PMS candidate members. This finding, together with the measured U excess, could be interpreted as due to the presence of accretion discs in their final evolutionary stages.

ACKNOWLEDGEMENTS

AJD is grateful for fruitful discussions with Anlaug Amanda Djupvik, Mayra Osorio, Enrique Macías and José Francisco Gómez. An anonymous referee is warmly acknowledged for accurate and improving comments. Based on data products from observations made with ESO Telescopes at the La Silla Paranal Observatory under programme ID 188.B-3002. These data products have been processed by the Cambridge Astronomy Survey Unit (CASU) at the Institute of Astronomy, University of Cambridge, and by the FLAMES/UVES reduction team at INAF/Osservatorio Astrofisico di Arcetri. These data have been obtained from the *Gaia*-ESO Survey Data Archive, prepared and hosted by the Wide Field Astronomy Unit, Institute for Astronomy, University of Edinburgh, which is funded by the UK Science and Technology Facilities Council.

This work was partly supported by the European Union FP7 programme through ERC grant number 320360 and by the Leverhulme Trust through grant RPG-2012-541. We acknowledge the support from INAF and Ministero dell' Istruzione, dell' Università' e della Ricerca (MIUR) in the form of the grant 'Premiale VLT 2012'. The results presented here benefit from discussions held during the *Gaia*-ESO workshops and conferences supported by the ESF (European Science Foundation) through the GREAT Research Network Programme.

This publication makes use of data products from the Two Micron All Sky Survey, which is a joint project of the University of Massachusetts and the Infrared Processing and Analysis Center/California Institute of Technology, funded by the National Aeronautics and Space Administration and the National Science Foundation.

This research has made use of the NASA/ IPAC Infrared Science Archive, which is operated by the Jet Propulsion Laboratory, California Institute of Technology, under contract with the National Aeronautics and Space Administration.

AJD, LS, EJA and MTC acknowledge financial support from the Spanish Ministerio de Economía y Competitividad, through grant AYA2013-40611-P. JLY acknowledges support from FCT (SFRH/BSAB/1423/2014 and UID/FIS/04434/2013). TM acknowledges financial support from Belspo for contract PRODEX GAIA-DPAC.

REFERENCES

Alcalá J. M. et al., 2014, A&A, 561, 2
Allen L. E. et al., 2004, ApJS, 154, 363
Andrews S. M., Rosenfeld K. A., Kraus A. L., Wilner D. J., 2013, ApJ, 771, 129
Balona L. A., 1994, MNRAS, 267, 1060 (B94)
Baume G., Vazquez R. A., Carraro G., Feinstein A., 2003, A&A, 402, 549 (B03)
Bell C. P. M., Rees J. M., Naylor T., Mayne N. J., Jeffries R. D., Mamajek E. E., Rowe J., 2014, MNRAS, 3496, 3511
Cabrera-Caño J., Alfaro E. J., 1985, A&A, 150, 298
Cameron L. M., 1985, A&A, 146, 59
Cantat-Gaudin T. et al., 2014, A&A, 569, 17
Carmona A. et al., 2014, A&A, 567, 51
Chené A. N. et al., 2012, A&A, 545, 54
Churchwell E. et al., 2009, PASP, 121, 213
Cottaar M., Hénault-Brunet V., 2014, A&A, 562, 20
Crawford D. L., 1975, AJ, 80, 955
de Winter D., Koulis C., The P. S., van den Ancker M. E., Perez M. R., Bibo E. A., 1997, A&AS, 121, 223
Dekker H., D'Odorico S., Kaufer A., Delabre B., Kotzlowski H., 2000, in Iye M., Moorwood A. F., eds, Proc. SPIE Conf. Ser. Vol. 4008, Optical and IR Telescope Instrumentation and Detectors. SPIE, Bellingham, p. 534
Delgado A. J., Alfaro E. J., Moitinho A., Franco J., 1998, AJ, 116, 1801
Delgado A. J., Alfaro E. J., Yun J. L., 2007, A&A, 467, 1397 (DAYI)
Delgado A. J., Alfaro E. J., Yun J. L., 2011, A&A, 531, 141 (DAYII)
Delgado A. J., Djupvik A. A., Costado M. T., Alfaro E. J., 2013, MNRAS, 435, 429
Dufton P. L. et al., 2006, A&A, 457, 265 (D06)
Drew J. et al., 2014, MNRAS, 440, 2036
Espaillat C. et al., 2014, in Beuther H., Klessen R. S., Dullemond C. P., Henning T., eds, Protostars and Planets VI. Univ. Arizona Press, Tucson, AZ, p.49
Feinstein A., Marraco H. G., 1980, PASP, 92, 266
Frasca A. et al., 2015, A&A, 575, 4
Geller A. M., Mathieu R. D., Braden E. K., Meibom S., Platais I., Dolan C. J., 2010, AJ, 139, 1383
Geller A. M., Latham D. W., Mathieu R. D., 2015, AJ, 150, 97
Gilmore G. et al., 2012, The Messenger, 147, 25
Guiglion G. et al., 2015, A&A, 583, 91
Gutermuth R. A., Megeath S. T., Myers P. C., Allen L. E., Pipher J. L., Fazio G. G., 2009, ApJS, 184, 18
Harmanec P., Bozic H., 2001, A&A, 369, 1140 (HB01)
Hauschildt P. H., Allard F., Baron E., 1999, ApJ, 512, 377
Herbst W., Miller D. P., 1982, AJ, 87, 1478 (H82)
Herczeg G. J., Hillenbrand L. A., 2008, ApJ, 681, 594
Hernandez J., Calvet N., Hartmann L., Briceño C., Sicilia-Aguilar A., Berlind P., 2005, AJ, 129, 856
Hillenbrand L. A., 2008, in Livio M., Sahu K., Valenti J., eds, A Decade of Extrasolar Planets around Normal Stars. Proc. STSci Symp. Ser. 19, p. 84
Hauck B., Mermilliod M., 1998, A&AS, 129, 431
Isella A., Testi L., Natta A., Neri R., Wilner D., Qi Ch., 2007, A&A, 469, 213
Jackson R. J. et al., 2015, A&A, 580, 75
Jeffries R. D. et al., 2014, A&A, 563, 94
Kalari et al., 2015, MNRAS, 453, 1026
Kim K. H. et al., 2013, ApJ, 769, 149
Lanzafame A. C. et al., 2015, A&A, 576, 80
Luhman K. L., Mamajek E. E., 2012, ApJ, 758, 31
Granato, G. L.Marigo P., Girardi L., Bressan A., Groenewegen M. A. T., Silva L., 2008, A&A, 482, 883
Moór A. et al., 2011, ApJS, 193, 4
Pasquini L., Avila G., Blecha A. et al., 2002, The Messenger, 110, 1
Pecaut M. J., Mamajek E. E., 2013, ApJS, 208, 9
Pecaut M. J., Mamajek E. E., Bubar E. J., 2012, ApJ, 746, 154
Gaia-ESO Consortium.Randich S., Gilmore G., 2013, The Messenger, 154, 47
Rebull L. M. et al., 2002, AJ, 123, 1528
Rigliaco E. et al., 2016, A&A, 588, 123
Sampedro L. M., Alfaro E. M., 2016, MNRAS, 457, 3949
Schuster W. J., Nissen P. E., 1989, A&A, 221, 65
Sicilia-Aguilar A., Hartmann L. W., Hernandez J., Briceño C., Calvet N., 2005, AJ, 130, 188
Siess L., Dufour E., Forestini M., 2000, A&A, 358, 593
Skrutskie M. F. et al., 2006, AJ, 131, 1163
Smiljanic R. et al., 2014, A&A, 570, 122
Spina L. et al., 2014, A&A, 567, 55
Suchkov A. A., Schultz A. B., Lisse C. M., 2002, ApJ, 570, L29 (S02)
Turner D. G., Grieve G. R., Herbst W., Harris W. E., 1980, AJ, 85, 1193 (T80)
Turner D. G., 1990, PASP, 102, 1331
Vasilevskis S., Klemola A., Preston G., 1958, AJ, 63, 387
Wolfe J. H., 1970, Multivariate Behav. Res., 5, 329
Zhao J.-l., Tian K.-p., Xu Z.-h., Yin M.-g., 1982, Chin. Astron. Astrophys., 6, 344

[1]*Instituto de Astrofísica de Andalucía (IAA-CSIC), Glorieta de la Astronomía, E-18008 Granada, Spain*

[2]*Instituto de Astrofísica e Ciências do Espaço, Universidade de Lisboa, OAL, Tapada da Ajuda, PT1349-018 Lisboa, Portugal*
[3]*Departament d'Astronomia i Meteorologia, Institut de Ciències del Cosmos (ICCUB), Universitat de Barcelona (IEEC-UB), Martí i Franquès 1. E-08028 Barcelona, Spain*
[4]*INAF-Osservatorio Astrofisico di Catania, via S. Sofia 78, I-95123 Catania, Italy*
[5]*Università di Catania, Dipartimento di Fisica e Astronomia, Sezione Astrofisica, via S. Sofia 78, I-95123 Catania, Italy*
[6]*School of Physics, Astronomy and Mathematics, University of Hertfordshire, College Lane, Hatfield, Hertfordshire AL10 9AB, United Kingdom*
[7]*Thüringer Landessternwarte, Sternwarte 5, D-07778 Tautenburg, Germany*
[8]*Royal Observatory of Belgium, Ringlaan 3, B-1180 Brussels, Belgium*
[9]*Université de Liège, Institut d'Astrophysique et de Géophysique, Allée du 6 Août, 17, B-4000 Liège 1, Belgium*
[10]*Geneva Observatory, University of Geneva, Maillettes 51, CH-1290 Sauverny, Switzerland*
[11]*INAF – Osservatorio Astrofisico di Arcetri, Largo E. Fermi 5, I-50125 Florence, Italy*
[12]*Astrophysics Group, Keele University, Keele, Staffordshire ST5 5BG, United Kingdom*
[13]*INAF – Osservatorio Astronomico di Palermo, Piazza del Parlamento 1, I-90134 Palermo, Italy*
[14]*INAF – Padova Observatory, Vicolo dell'Osservatorio 5, I-35122 Padova, Italy*
[15]*Armagh Observatory, College Hill, Armagh BT61 9DG, United Kingdom*
[16]*Institute of Astronomy, University of Cambridge, Madingley Road, Cambridge CB3 0HA, United Kingdom*
[17]*European Southern Observatory, Alonso de Cordova 3107 Vitacura, Santiago de Chile, Chile*
[18]*Astrophysics Research Institute, Liverpool John Moores University, 146 Brownlow Hill, Liverpool L3 5RF, United Kingdom*
[19]*Departamento de Ciencias Fisicas, Universidad Andres Bello, Republica 220, Santiago, Chile*
[20]*Instituto de Astrofísica e Ciências do Espaço, Universidade do Porto, CAUP, Rua das Estrelas, P-4150-762 Porto, Portugal*

This paper has been typeset from a TEX/LATEX file prepared by the author.